Advances in Radiation Oncology (2025) **10**, 101821

advances in radiation oncology

www.advancesradonc.org

Scientific Article

Comparative Analysis of ^{68}Ga-Prostate-Specific Membrane Antigen Positron Emission Tomography/Computed Tomography and Multiparametric Magnetic Resonance Imaging for Gross Tumor Volume Delineation in Radiation Therapy Planning of Prostate Cancer

Hamed Bagheri, PhD,[a] Seied Rabi Mahdavi, PhD,[b,*] Parham Geramifar, PhD,[c] Ali Neshasteh-Riz, PhD,[a] Masoumeh Sajadi-Rad, MD,[a] Habibollah Dadgar, PhD,[d] Hossein Arabi, PhD,[e] and Habib Zaidi, PhD[e,f,g,h,*]

[a]Radiation Biology Research Center, Iran University of Medical Sciences (IUMS), Tehran, Iran; [b]Department of Medical Physics, Radiation Biology Research Center, Iran University of Medical Sciences (IUMS), Tehran, Iran; [c]Department of Nuclear Medicine, School of Medicine, Shariati Hospital, Tehran, Iran; [d]Nuclear Medicine and Molecular Imaging Department, Imam Reza Research Center, RAZAVI Hospital, Mashhad, Iran; [e]Division of Nuclear Medicine and Molecular Imaging, Geneva University Hospital, Geneva, Switzerland; [f]Department of Nuclear Medicine and Molecular Imaging, University Medical Center Groningen, University of Groningen, Groningen, The Netherlands; [g]Department of Nuclear Medicine, University of Southern Denmark, Odense, Denmark; and [h]University Research and Innovation Center, Óbuda University, Budapest, Hungary

Received 16 August 2024; accepted 27 May 2025

Purpose: Magnetic resonance imaging (MRI) with multiparametric assessment is a cornerstone in radiation therapy planning for primary prostate cancer (PCa), offering the potential for focal dose escalation to dominant intraprostatic lesions to enhance PCa management. The prostate-specific membrane antigen (PSMA), which is frequently overexpressed in PCa, has led to the development of ^{68}Ga-labeled PSMA inhibitors for positron emission tomography (PET)/computed tomography (CT), showing promising results in PCa detection. This study aimed to conduct a comparative analysis of ^{68}Ga-PSMA PET/CT and multiparametric MRI (mpMRI) in delineating the gross tumor volume (GTV) in PCa.

Methods and Materials: A retrospective analysis was performed on 25 PCa patients who underwent ^{68}Ga-PSMA PET/CT and mpMRI at 2 distinct centers. The GTVs were delineated on MRI (GTV-MRI) by 2 nuclear medicine physicians and 1 radiation oncologist independently, while the GTVs based on PET/CT (GTV-PET) were outlined by 2 nuclear medicine physicians. The laterality (left, right, and bilateral) prostate lobes on mpMRI and PET/CT was assessed. To account for registration uncertainties, both GTV-PET and GTV-MRI were expanded isotropically by 5 mm to form the planning target volume (PTV), and the overlap between specific PTVs and their corresponding GTVs was quantified.

Sources of support: This work was supported by the Swiss National Science Foundation under grant SNSF 320030_231742 and Geneva League Against Cancer under grant LGC 2402.

Data Statement: It is the policy of our institution not to share clinical data owing to ethical and privacy restrictions.

*Corresponding authors: Seied Rabi Mahdavi, PhD; Email: Mahdavi.r@iums.ac.ir and Habib Zaidi, PhD; Email: habib.zaidi@hug.ch.

https://doi.org/10.1016/j.adro.2025.101821

Results: The average ± SD GTV-MRI and GTV-PET were 5.468 ± 11.6 cm^3 and 11.136 ± 14.3 cm^3, respectively, with the GTV-PET being significantly larger than the GTV-MRI (P = .003). GTV-MRI exhibited an intersection with GTV-PET of 3.5 ± 6.0 cm^3. The PTV derived from PSMA PET/CT encompassed 62% ± 27% of the GTV-MRI, with 44.4% of patients having the PTV covering 100% of the GTV-MRI. Conversely, the PTV based on GTV-MRI covered 50% ± 31% (mean ± SD) of the GTV-PET.
Conclusions: ^{68}Ga-PSMA PET/CT and mpMRI demonstrated consistent outcomes in 47% of patients (40%-54% of lesions). Notably, the GTV-PET was larger than the GTV-MRI, indicating a potential role for ^{68}Ga-PSMA PET/CT in radiation therapy planning for targeted radiation delivery to PCa.

Introduction

Accurate identification and delineation of the gross tumor volume (GTV) within the prostate gland are of utmost importance in the effective administration of radiation therapy (RT) for individuals diagnosed with prostate cancer (PCa). The size and extent of the tumor within the prostate, including factors such as infiltration into the seminal vesicles, play a significant role in determining the stage of the disease and subsequently classifying the patient into a specific risk group.[1,2] This information directly influences the planning of RT strategies, affecting decisions regarding androgen deprivation therapy (ADT) and the definition of clinical target volumes. Moreover, a precise definition of the intraprostatic GTV is particularly relevant for focal RT because comprehensive coverage of the GTV is crucial for the success of such targeted approaches.

In recent years, there has been a growing interest in this aspect, with multiparametric magnetic resonance imaging (mpMRI) currently considered the gold standard for detecting and segmenting the intraprostatic GTV.[3] Histopathological comparisons have demonstrated that the integration of anatomic and functional magnetic resonance imaging (MRI) data, such as T2-weighted spin echo imaging, dynamic contrast-enhanced (DCE) MRI, and diffusion-weighted imaging (DWI), enables the accurate identification of primary PCa. The use of 1.5 or 3T mpMRI for the detection of intraprostatic lesions has been linked to sensitivities ranging from 80% to 88% and specificities ranging from 89% to 100%, as reported in various studies.[4-6] However, previous studies have suggested that mpMRI might underestimate the actual GTV and fail to detect clinically significant lesions.[7,8] Simultaneously, positron emission tomography (PET) with prostate-specific membrane antigen (PSMA)-labeled tracers has emerged as a valuable technique for staging both primary and recurrent PCa.[9-12]

Eder et al[13] created a hybrid molecule by merging the PSMA binding motif from a urea-based PSMA inhibitor with a gallium chelator. The latter displays superior specific internalization in PCa cells when contrasted with dodecane tetraacetic acid) conjugates. In clinical trials, ^{68}Ga-PSMA PET/computed tomography (CT) has exhibited significant promise in diagnosing recurrent PCa.[14,15] ^{68}Ga-PSMA PET/CT exhibited a superior detection rate for recurrent PCa lesions in comparison with ^{18}F-choline-PET/CT.[16] Rowe et al[17] demonstrated in a recent study that N-[N-[(S)-1,3-dicarboxypropyl] carbamoyl]-4-[18F]fluorobenzyl-L-cysteine (^{18}F-DCFBC PET/CT) has the ability to detect a greater number of clinically significant high-grade tumors with increased specificity compared with MRI. The study also noted a relatively low PSMA expression in benign prostatic lesions. However, the sensitivity of ^{18}F-DCFBC PET/CT for primary PCa was found to be lower than that of MRI.

Recent advances have highlighted the potential role of PSMA PET/CT not only as a complement to mpMRI for intraprostatic tumor localization but also as a valuable tool for treatment planning, particularly in focal microboost strategies. Furthermore, in postoperative settings where MRI may be limited due to anatomic distortion or fibrosis, PSMA PET/CT can assist in identifying localized recurrence and guiding focal salvage RT.[18]

Although PSMA PET provides superior sensitivity for detecting lymph node metastases, particularly in high-risk and recurrent PCa cases, MRI remains indispensable for local tumor characterization. PSMA PET has become the standard of care for biochemical recurrence due to its ability to detect lesions at low prostate-specific antigen (PSA) levels, while mpMRI provides detailed anatomic resolution for intraprostatic lesion delineation. The 2 modalities are complementary, and their integration, for instance, through PSMA PET/MRI fusion, can enhance target definition and guide personalized RT planning.[19]

Contemporary imaging methods need to meet specific requirements in order to assist radiation oncologists in planning treatments, including the precise staging of both extraprostatic and intraprostatic tumor masses, the reliable outlining of the intraprostatic GTV, and the consistent identification of the biological characteristics of PCa. This analysis explores the capability of existing imaging methods, with a focus on mpMRI and PSMA PET, to meet these criteria. This study aimed to conduct a comparative analysis of ^{68}Ga-PSMA PET/CT and mpMRI in delineating the GTV in PCa. To achieve this, patients from 2 distinct medical facilities were enrolled, and established contouring methods were used for GTV delineation.[20,21]

Methods and Materials

Data acquisition

This study enrolled individuals from 2 health care facilities, covering the timeframe between July 2020 and September 2021. At center 1, a total of 18 patients diagnosed with PCa were included in the retrospective study. These patients underwent both ^{68}Ga-PSMA PET/CT and mpMRI. Prior therapeutic interventions, such as ADT or transurethral prostate resection, were taken into consideration, and there was a minimum time gap of 90 days between the PSMA PET and the MRI scan. Similarly, at center 2, 7 patients with PCa were recruited for the study. These patients underwent ^{68}Ga-PSMA PET/CT and 1.5T MRI. It is important to note that all patients from both centers provided written informed consent for their participation in the study.

MRI

Center 1

Prostate magnetic resonance (MR) images were acquired on either a 3T system (Trio Tim; Siemens) or a 1.5T system (Espree, Aera, and Avanto; Siemens). The MRI protocol was as follows: T2-weighted turbo spin echo images with repetition time (TR) 5500 ms (3T)/8650 to 9400 ms (1.5T); echo time (TE) 103 to 108 ms (3T)/111 to 119 ms (1.5T); field-of-view (FOV) 150 × 150 mm; slice thickness 3 mm without gap; matrix 192 × 192. DWI was performed with an echo planar imaging sequence in transverse orientation with TR 3500 ms (3T)/2800 to 3840 ms (1.5T); TE 73 ms (3T)/61 to 87 ms (1.5T); flip angle 90°; FOV 250 × 250 mm (3T)/300 × 300 to 400 × 338 (1.5T); slice thickness 3 mm (3T)/3 to 6 mm (1.5T); slice gap 0 mm (3T)/0 to 1.5 mm (1.5T); matrix 160 × 160 (3T)/192 × 162 to 160 × 160 (1.5T), b values 50, 400, and 800 s/mm^2 (3T)/0, 100, 400, and 800 or 0, 250, 500, and 800 s/mm^2 (1.5T). DCE-MRI was acquired with dynamic 3-dimensional fast low-angle shot sequence in transverse orientation with TR 5.13 ms (3T)/4.65 to 4.1 ms (1.5T); TE 2.45 ms (3T)/1.58 to 1.6 ms (1.5T); flip angle 12° (3T)/12° to 15° (1.5T); FOV 260 × 260 mm (3T)/260 × 260 to 400 × 387 (1.5T); partition thickness 3 mm (3T)/2 to 3 mm (1.5T); matrix 192 × 192 (3T)/192 × 192 to 384 × 372 (1.5T).

Center 2

The hybrid system includes a built-in MRI system capable of generating a magnetic field intensity of 1.5T MRI (MAGNETOM Trio Tim, Siemens). T1-weighted (T1W) imaging, T2-weighted (T2W) imaging, and diffusion weighted (DW) imaging (b = 100, 500, 1000, and 1500 s/mm^2) of the prostate and pelvis were simultaneously acquired. The apparent diffusion coefficient (ADC) was calculated from DWI. T1WI sequence parameters were as follows: TR/TE = 5.04/2.24 ms, 4 mm slice thickness, 20% interslice gap, 350 mm × 350 mm FOV, and a 256 × 256 matrix. The axial fast spin echo T2WI sequence parameters were as follows: TR/TE = 3998/88.74 ms, 6 mm slice thickness, 20% interslice gap, 300 mm × 300 mm FOV, and a 320 × 320 matrix.

PET/CT imaging

Center 1

A standardized protocol was employed, where all patients followed a minimum fasting period of 4 hours before the administration of the radiopharmaceutical. Patients were also instructed to empty their bladders prior to the PET scan. The average ± SD activity of ^{68}Ga-PSMA administered was 172 ± 34 MBq. Following injection, patients underwent whole-body PET scans after a 1-hour interval. To correct for attenuation, low-dose CT scans (120 kVp and 25 mAs) were performed concurrently with the PET scans. These scans were conducted on 18 patients using a 64-slice Vereos PET/CT scanner, with the necessity for CT determined based on prior scans and any contraindications. The uptake of ^{68}Ga-PSMA was quantified using standardized uptake values (SUVs), providing a measure of the regional concentration of the tracer normalized by the injected dose and the patient's body weight.

Center 2

Whole-body PET scans were conducted using ^{68}Ga-PSMA, commencing 1 hour postinjection. The median injected activity was 313 MBq, ranging between 245 and 454 MBq. These scans were performed on 7 patients using a 6-slice True-Point Siemens PET/CT scanner. To correct for attenuation, low-dose CT scans (120 kVp and 30 mAs) were performed concurrently with the PET scans. Regarding the standard operating procedure of the different centers, various amounts of activities were injected depending on the sensitivity of the PET scanners to detect the small involved lesions.

GTV delineation

The prostate volume was delineated by a board-certified radiologist/board-certified radiation oncologist with more than 6 years of experience in the interpretation of the prostate on both CT and MR images following the guidelines outlined by the European Society for Radiotherapy and Oncology and the Advisory Committee on Radiation Oncology Practice.[22] The T2-weighted attenuation-corrected PET and CT data sets for each patient were imported into the radiation treatment planning

system (RayStation Laboratories). Initially, automatic matching of axial T2-weighted MRI and CT images was performed using mutual information registration in all 3 dimensions. In cases where anatomic discrepancies were observed during visual assessment, manual adjustments were made based on anatomic information of the prostatic gland. The default registration of CT and PET images was then applied, with manual modifications implemented as necessary to address any anatomic inconsistencies. The GTV based on PET data sets (GTV-PET) was delineated by 2 nuclear medicine physicians and 1 radiation oncologist. The presence of PCa on PET/CT images was defined as any monofocal or multifocal uptake exceeding adjacent background uptake in more than 1 slice within the CT-defined prostate gland (Fig. 1).[22] During the interpretation of PET images, both uncorrected and attenuation-corrected images were assessed concurrently to verify the existence of artifacts such as contrast, metal implants, or patient repositioning. Additionally, it was essential to modify the display window width and level of the image to accurately visualize the PSMA-ligand uptake site or neighboring high-uptake organs, such as the kidney, ureter, or bladder. Zamboglou et al[23] demonstrated that employing the same window level ($SUV_{min-max}$, 0-5) can minimize interobserver variability in GTV delineation using ^{68}Ga-PSMA PET. They also suggested that establishing a fixed optimal window level could enhance consistency in ^{18}F-PSMA PET.[23] Consequently, to prevent any potential bias among observers, a uniform fixed window position was adopted for each observer in this study. The interpretations of all images were validated by an experienced nuclear medicine physician. Two nuclear medicine physicians and 1 radiation oncologist, specializing in PCa, examined the images and independently outlined the target area of all suspected visible tumors. Notably, GTVs based on MRI, PET, and PET/MRI were accessible for each patient in this particular case. During the process of GTV based on MRI (GTV-MRI) delineation, physicians used a combination of T1WI, T2WI, and DWI images, which included ADC images, to identify the locations of lesions. In terms of PCa lesions, they appeared relatively hypointense on T1WI images, exhibited a similar level of hypointensity on T2WI images, and displayed high signal intensity on DWI images, accompanied by low ADC values. Following the exclusion of inflammatory or benign lesions (described in Appendix E1), the determination of PCa was made based on the integration of multisequence images. Ultimately, the 2 nuclear medicine physicians and 1 radiation oncologist obtained the GTV-MRI through manual contouring on axial T2WI MRI. Two different approaches were employed to contour the PSMA PET

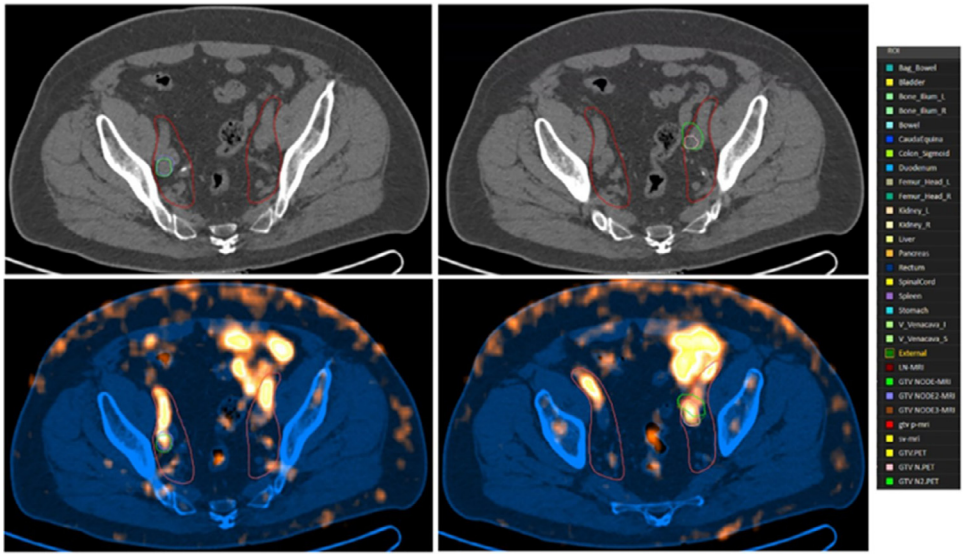

Figure 1 Correlation between tumor volumes depicted on multimodal images and dose distribution. A representative clinical example of ^{68}Ga-prostate-specific membrane antigen positron emission tomography (PET) guided intensity modulated radiation therapy (IMRT) of a patient with positive lymph nodes. A 74-year-old patient presenting with primary prostate cancer, with a Gleason score of 9 (4 + 5), an initial prostate-specific antigen (PSA) of 15 ng/mL, and cT3b stage. The patient had a 60% chance of lymph node involvement. Top panel: computed tomography revealed gross tumor volumes (GTVs) for 1 lymph node in the left pelvis (red contours indicate clinical target volumes in the lymph nodes, and green contour indicates GTVs for the involved lymph node). Bottom panel: GTVs for 1 lymph node in the right pelvis (red contours indicate clinical target volumes in the lymph nodes, and green contour indicates GTVs for the involved lymph node) from ^{68}Ga-prostate-specific membrane antigen PET/computed tomography images. The patient had neoadjuvant androgen deprivation therapy in combination with IMRT and image guided radiation therapy: 76 Gy to the prostate, 45 Gy to the pelvic lymph nodes, and a sequential boost to the 2 PET-positive lymph nodes with up to 54 Gy. In the right panel, the dose wash representation of the IMRT plan is shown. MRI = magnetic resonance imaging, L= left, R = right. LN = lymph node.

images. First, the GTV-PET was delineated based on visual analysis of the PET images. This method involved identifying areas where the PSMA uptake was significantly higher than the surrounding normal tissue background, indicating the presence of metabolic abnormalities and suspected lesions. Additionally, the longest tumor length in PET was determined by measuring the maximum diameter of the target area along the maximum axis plane. Second, the GTV-PET values were obtained using a contour method with SUV_{max}. This involved quantifying the PSMA uptake (ie, SUV) and then determining the percentage of SUV in each voxel by measuring the highest SUV in the corresponding prostate. The GTV-PET/MRI was obtained through manual delineation after the integration of PET images with T2WI axial images. Lesions exhibiting elevated local radioactive uptake within the prostate gland compared with surrounding normal tissues, along with the aforementioned MRI features, were identified as positive lesions.

The GTVs were manually delineated in each slice. Specifically, the GTV-MRI T2-weighted data sets were outlined separately by 2 nuclear medicine physicians and 1 radiation oncologist. These contouring experts had access to comprehensive MRI data sets, including side-by-side DCE and DWI data. The criteria for lesion identification involved assessing hypointensity on the T2-weighted image alongside lesion presence on either the DWI or DCE image, or both, at the same location to confirm positivity.[24] For the GTV definition, the primary reference was the ADC maps derived from the DWI data. Additionally, the postinjection time frame displaying maximum contrast within the prostate was manually selected from the DCE time series. Following this, all GTVs were registered to the PET data set, and the SUV_{max} within the volumes of interest was measured. To mitigate background signaling, delineation of the bladder was performed, and if necessary, it was excluded from both GTV-MRI and GTV-PET delineations.

Statistical analysis

Statistical analysis was conducted using GraphPad Prism v8.4.2 (GraphPad Software). The normality of the distribution was assessed using the D'Agostino and Pearson normality test. To compare metric variables that were not normally distributed, a Wilcoxon matched-pairs signed-rank test was employed. On the other hand, a paired *t* test was used to compare normally distributed metric variables. For categorical variables, a 1-sided Fisher's exact test was used. The significance level was set at .05. The figures presented in this study were generated using GraphPad Prism v8.4.2 (GraphPad Software). For further statistical analysis, the Mann-Whitney *U* test, Wilcoxon signed-ranked test, exact significance (2-tailed, derived from 1-tailed significance), and asymptotic significance (2-tailed) were used to compare the GTV volume (cm^3) between the MRI and PET groups. In the ranks section, both groups had 25 observations each.

Results

From July 2020 to September 2021, a total of 25 individuals diagnosed with primary PCa underwent mpMRI of the pelvis and ^{68}Ga-PSMA PET/CT scans within a 3-month timeframe (an example is shown in Fig. 2). The average age of these patients was 68.6 years (SD, 7.9 years). The majority of the patients fell under the intermediate-risk category based on the D'Amico classification. Prior to the imaging procedures, PSA levels were assessed, revealing a mean PSA level of 21.4 ng/mL (median ± SD, 11.64 ± 19.7 ng/mL). The characteristics of the GTVs based on the PET and MRI data sets are shown in Table E1. The median GTV obtained from the PET data sets (GTV-PET, 4.16 cm^3) was larger than the median GTV obtained from the MRI T2-weighted data sets. The difference between GTV-PET and GTV-MRI was significant ($P = .003$).

For the 18 cases from center 1, mpMRI was able to identify 31 intraprostatic GTVs, whereas PET detected 53. When considering individual patients, the median number of GTVs detected by mpMRI and PET was 2 (range, 1-5) and 3 (range, 1-8), respectively ($P < .01$). The median volume of GTV-MRI and GTV-PET per patient was 2.1 mL (range, 0.2-42.8) and 3.7 mL (range, 0.4-85), respectively ($P < .01$). For the 7 cases from center 2, the median volume of GTV-MRI and GTV-PET per individual was 3.8 mL (range, 0.1-59.5) and 4.4 mL (range, 2.1-60.1), respectively ($P = .02$) (Table E1).

Additionally, the results of the analyses exhibited that patients with a higher Gleason score (GS) tended to have higher SUV_{max} values on PET/CT scans, indicating a potential correlation between the aggressiveness of PCa and the metabolic activity detected on imaging. Furthermore, the study also revealed that patients with larger GTVs on MRI tended to have higher SUV_{max} values on PET/CT scans, suggesting that tumor volume may also play a role in the uptake of radiotracers in PCa. Overall, the findings of this study highlight the importance of considering multiple factors, including PSA level, GS, and tumor volume, when interpreting imaging results in patients with PCa. The average ± SD functional tumor volume for MRI (ie, GTV-MRI) and PET (ie, GTV-PET) was 5.468 ± 11.6 cm^3 and 11.136 ± 14.3 cm^3, respectively (Tables E1-E3).

High-risk patients (n = 8), defined as those with a PSA > 20, represent the most aggressive disease profile. These patients typically require intensive treatment, such as ADT combined with radiation or surgery (Table E4). Intermediate-risk patients (n = 6), defined as those with a PSA of 10 to 20, indicate moderate disease severity.

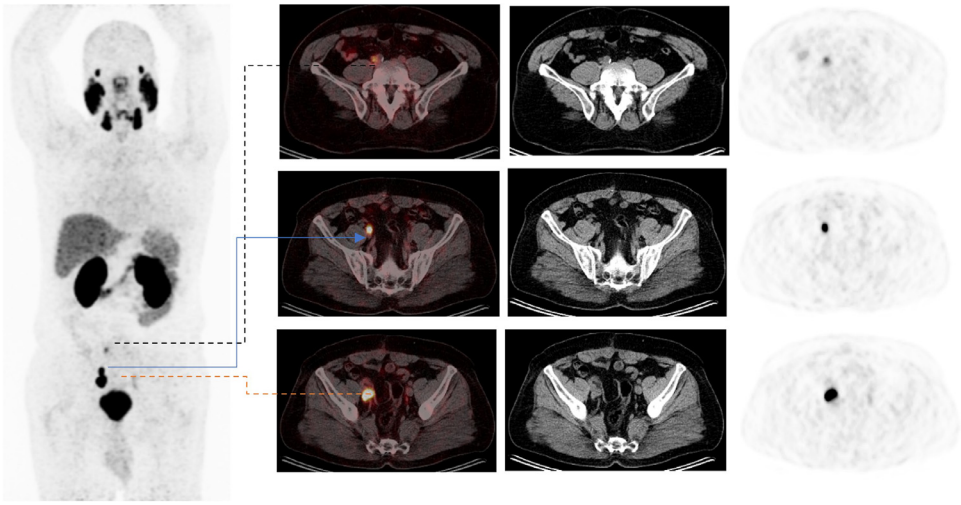

Figure 2 A 71-year-old prostate cancer patient who underwent prostatectomy. The involved pelvic lymph nodes were treated with radiation therapy. The involved paraortic lymph nodes were treated with abiraterone and Zoladex (TerSera Therapeutics). Prostate-specific antigen (PSA) was 3.24 before ^{68}Ga-prostate-specific membrane antigen positron emission tomography. There was a lymph node (11 mm in diameter) at the right side of the aorta with an maximum standardized uptake value (SUV_{max}) of 15.63.

Management may include active surveillance, radiation, or ADT based on additional clinical factors. Low-risk patients (n = 11), defined as those with a PSA < 10, suggest less aggressive disease. These patients may be candidates for active surveillance or localized therapy. The majority of patients in this cohort (11/25, 44%) fell into the low-risk category, while high-risk cases (32%) still represented a significant proportion. This distribution underscores the importance of risk-adapted treatment strategies in line with the National Comprehensive Cancer Network (NCCN) guidelines.

There was no significant difference in the mean age between the group with a Gleason score ≤7 and the group with a Gleason score >7. The total PSA level was significantly elevated in the group with a Gleason score >7 compared with the group with a Gleason score ≤ 7 (P = .001). Similarly, the PSMA SUV_{max} levels were significantly higher in the group with a Gleason score > 7 than in the group with a Gleason score ≤7 (P = .03). Tables E5 and E6 provide further evidence supporting these findings. We also identified relationships between PSA and other variables. In this study, a positive correlation was found between PSMA SUV_{max} and total PSA (r = 0.260, P = .01). Similarly, a positive correlation was observed between PSMA SUV_{max} and the Gleason score (r = 0.260, P = .01). Additionally, a positive correlation was noted between total PSA and the Gleason score (r = 0.320, P = .001).

In summary, both PSMA SUV_{max} and total PSA levels were elevated in the group with higher Gleason scores. A positive correlation was observed between PSMA SUV_{max} and total PSA. Clinicians should exercise caution in such cases because the likelihood of metastasis is greater in groups with high Gleason scores. Based on the findings of this study, it is suggested that ^{68}Ga-PSMA PET/CT imaging should be routinely incorporated for staging in medium- to high-risk patients. Furthermore, considering the relationship between the ^{68}Ga-PSMA PET/CT findings, SUV_{max} values, histopathological results, and laboratory data, SUV_{max} values can also serve as a prognostic indicator.

Additionally, the results of the analyses exhibited that patients with a higher GS tended to have higher SUV_{max} values on PET/CT scans, indicating a potential correlation between the aggressiveness of PCa and the metabolic activity detected on imaging (Table E7). A significant positive correlation was found between PSMA SUV_{max} and total PSA (P = .01). A positive correlation was observed between PSMA SUV_{max} and the Gleason score (P = .01). A positive correlation was observed between total PSA and the Gleason score (P = .001).

Figure 3 compares the GTV and planning target volume (PTV) in a clinical example of ^{68}Ga-PSMA PET guided intensity modulated RT (IMRT) in a 71-year-old patient presenting with primary PCa, with a Gleason score of 9 (4 + 5), an initial PSA of 12 ng/mL, and cT3b stage. The patient had neoadjuvant ADT in combination with IMRT with 76 Gy to the prostate, 45 Gy to the pelvic lymph nodes, and a sequential boost to the 2 PET-positive lymph nodes with up to 54 Gy.

As discussed earlier in the GTV delineation section, the comparison of the GTVs defined on MRI/CT/PET in a clinical example of ^{68}Ga-PSMA PET guided IMRT in a 69-year-old patient presenting with primary PCa, with a Gleason score of 8 (4 + 4), an initial PSA of 13 ng/mL, and cT3b stage, is shown in Fig. 4. Moreover, a 5 mm margin was implemented to account for uncertainties in the registration of PSMA to its associated CT. This margin was established with consideration of potential discrepancies that may arise during

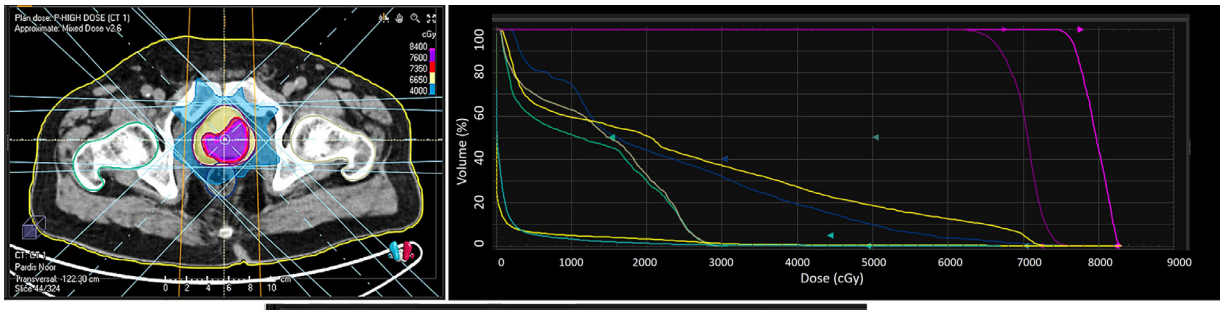

Function	Constraint	Dose	ROI	Description	Weight	Value
Physical Composite Objective						0.0133
Min Dose		Plan	PTV 70-HIGH DOSE	Min Dose 6800 cGy	20.00	0.0037
Max Dose		Plan	PTV 70-HIGH DOSE	Max Dose 7200 cGy	20.00	0.0017
Max DVH		Plan	Bladder	Max DVH 3000 cGy to 40% volume	5.00	0.0000
Max DVH		Plan	Rectum	Max DVH 3000 cGy to 40% volume	5.00	0.0000
Max Dose		Plan	Bag_Bowel	Max Dose 4900 cGy	5.00	2.6492E-4
Max DVH		Plan	Bag_Bowel	Max DVH 4400 cGy to 5% volume	5.00	0.0000
Max DVH		Plan	Femur_Head_L	Max DVH 1500 cGy to 50% volume	2.00	0.0000
Max DVH		Plan	Femur_Head_R	Max DVH 1500 cGy to 50% volume	2.00	0.0000
Max Dose		Plan	ring PET 1-15mm	Max Dose 7000 cGy	2.00	6.3740E-4
Max DVH		Plan	ring PET 1-15mm	Max DVH 5000 cGy to 50% volume	2.00	0.0057
Min Dose		Plan	GTV PET HIGH DOSE	Min Dose 7800 cGy	20.00	0.0013
Max Dose		Plan	GTV PET HIGH DOSE	Max Dose 8200 cGy	10.00	2.8162E-5

Figure 3 Comparison of the gross tumor volume (GTV) and planning target volume (PTV) in a representative clinical example of ^{68}Ga-prostate-specific membrane antigen positron emission tomography (PET) guided intensity modulated radiation therapy (IMRT) in a prostate cancer patient. A 71-year-old patient presenting with primary prostate cancer, with a Gleason score of 9 (4 + 5), an initial prostate-specific antigen (PSA) of 12 ng/mL, and cT3b stage. The patient had neoadjuvant androgen deprivation therapy, in combination with IMRT, with 76 Gy to the prostate, 45 Gy to the pelvic lymph nodes, and a sequential boost to the 2 PET-positive lymph nodes with up to 54 Gy. Right panel: the dose-volume histogram (DVH) of the IMRT plan. The bottom panel shows the optimization constraints and objectives for IMRT planning (regions of interest (ROIs), dose constraints [eg, minimum {Min} and maximum {Max} doses and DVH constraints], and weights).

the fusion of MRI with CT data derived from PET scans. While we acknowledge that the FLAME study employed a zero margin, our choice to adopt a 5 mm margin is grounded in the existing literature, which emphasizes the importance of incorporating margins to mitigate registration errors.

SUV_{max} values for GTV-PET and GTV-MRI were assessed in a cohort of 12 out of 25 patients, with SUV_{max} of the GTV-PET found to be situated within the GTV-MRI. The median SUV_{mean} was observed to be greater in GTV-MRI (7.45) than in GTV-PET (5.94), yielding a P value of .042. The findings revealed that the median SUV_{mean} in GTV-MRI was significantly higher than that in GTV-PET. The P value of .042 indicates that the observed difference was statistically significant (Fig. 5).

Considering uncertainties in registration, both GTV-PET and GTV-MRI were expanded isotopically by 5 mm to form a PTV. Moreover, the overlap between PTVs drawn on PET or MR images and their corresponding GTVs defined on MR or PET images (from the opposite modality) was quantified. The PTV derived from PSMA PET/CT encompassed 62% ± 27% of the GTV-MRI, with 44.4% of patients having a PTV that covered 100% of the GTV-MRI. Conversely, the PTV based on GTV-MRI covered 50% ± 31% of GTV-PET.

Table 1 presents the characteristics of the GTV-PET and GTV-MR data sets. The median GTV obtained from the PET data sets (GTV-PET = 4.16 cm^3) was larger than the median GTV obtained from the T2-weighted MRI data sets. The difference between GTV-PET and GTV-MRI was significant (P = .003). Table E3 shows the subgroup analysis based on ^{68}Ga-PSMA PET/CT versus mpMRI and ^{68}Ga-PSMA PET versus mpMRI in detecting bilateral lesions and seminal vesicle invasion for PCa.

The average rank for the MRI group was 21.58, while it was 29.42 for the PET group, indicating that PET data generally have higher ranks compared with MRI. The total ranks for MRI and PET were 539.50 and 735.50, respectively. In the test statistics, the Mann-Whitney U statistic was 214.5, reflecting the rank differences between the 2 groups, whereas the Wilcoxon W statistic was 539.5, representing the total ranks for the MRI group. The standardized z value was −1.902, with a significance level (P value) of .057 (Table E8). This P value indicates that the observed difference in GTV volume (cm^3) between the MRI and PET groups is not statistically significant at the 5% level. In other words, we cannot confidently reject the null hypothesis, which states that there is no significant difference between the 2 groups. However, the P value is close to the significance threshold, suggesting a potential difference that might be explored further with a larger sample size or adjusted test conditions. Overall, the results show that the average ranks of PET are higher than those of MRI, which could suggest that the GTV volume (cm^3) is, on average, larger in the PET group. Nevertheless, this difference cannot be confirmed statistically, highlighting the need for further investigation and possibly additional analyses.

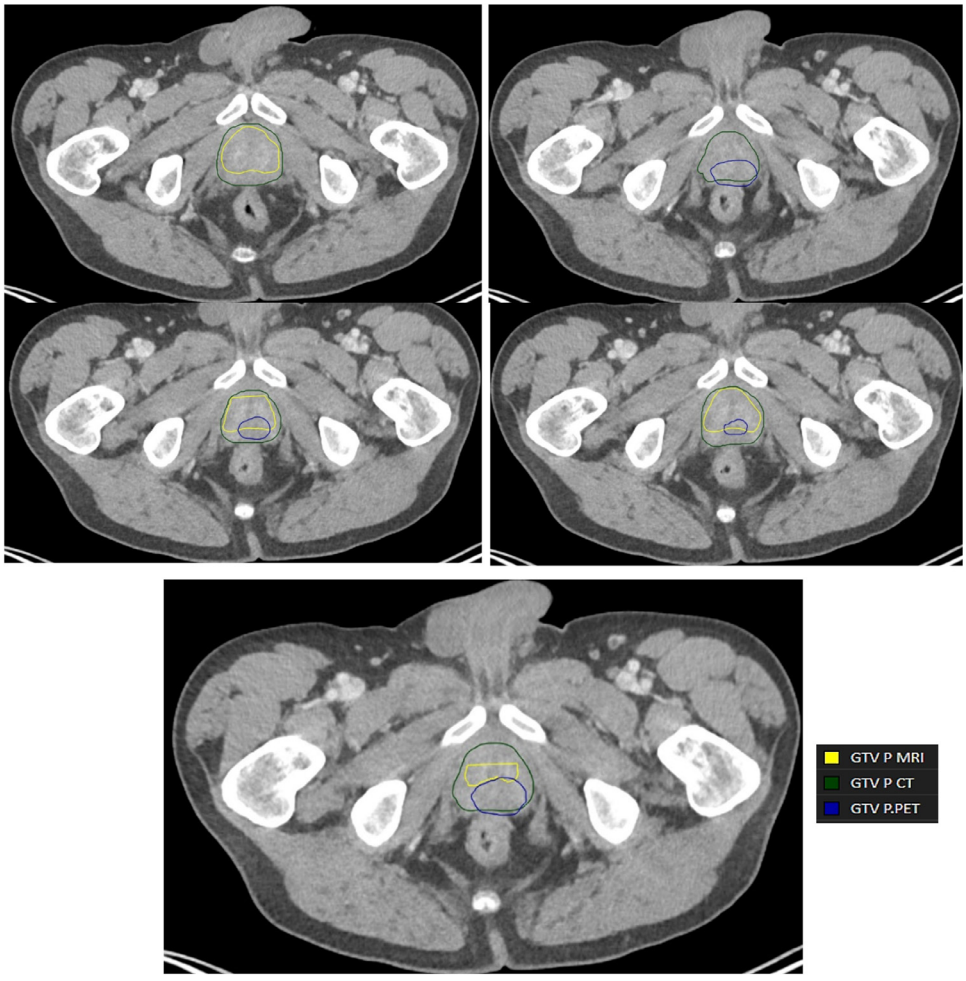

Figure 4 Comparison of the gross tumor volumes (GTVs) for magnetic resonance imaging (MRI)/computed tomography (CT)/positron emission tomography (PET) in a clinical example of ^{68}Ga-prostate-specific membrane antigen PET guided intensity modulated radiation therapy in a prostate cancer patient. A 69-year-old patient presenting with primary prostate cancer, with a Gleason score of 8 (4 + 4), an initial prostate-specific antigen (PSA) of 13 ng/mL, and cT3b stage.

A comparative analysis of the 18 cases from center 1 revealed that PSMA PET detected significantly more intraprostatic lesions than mpMRI (53 vs 31 GTVs). The per-patient evaluation demonstrated higher lesion detection by PET (median, 3; range, 1-8) versus MRI (median, 2; range, 1-5; $P < .01$), with correspondingly larger median tumor volumes (3.7 mL vs 2.1 mL; $P < .01$) (Table E9). This pattern was maintained in the 7 cases from center 2 (PET: 4.4 mL vs MRI: 3.8 mL; $P = .02$). Notably, elevated Gleason scores correlated with increased SUV_{max} values ($P < .05$), reflecting greater metabolic activity in more aggressive tumors. Similarly, larger MRI-derived tumor volumes were associated with higher radiotracer uptake ($P < .05$). These results emphasize the multifactorial interpretation of PCa imaging, where the integration of PSA levels, histopathological grade, and volumetric parameters enhances diagnostic accuracy (Table E10).

The average ranks indicate that center 2 had slightly higher GTV values for both MRI and PET compared with center 1. However, these differences were minimal and not statistically significant (P values $> .05$). The Mann-Whitney U test results confirmed that the hypothesis of a significant difference between the 2 centers can be rejected. Therefore, it can be concluded that GTV values (cm^3) do not show a substantial difference between these 2 centers. For a more detailed analysis, increasing the sample size or using alternative statistical methods might be beneficial.

The accuracy and interreader agreement results for PSMA PET and mpMRI for the detection of PCa are shown in Table E11.

Discussion

mpMRI is considered the primary method for detecting PCa[3] and identifying important lesions, as local recurrences usually happen at the location of primary tumor lesions identified through mpMRI.[23,24] However, research by Priester et al[8] revealed that mpMRI tends to

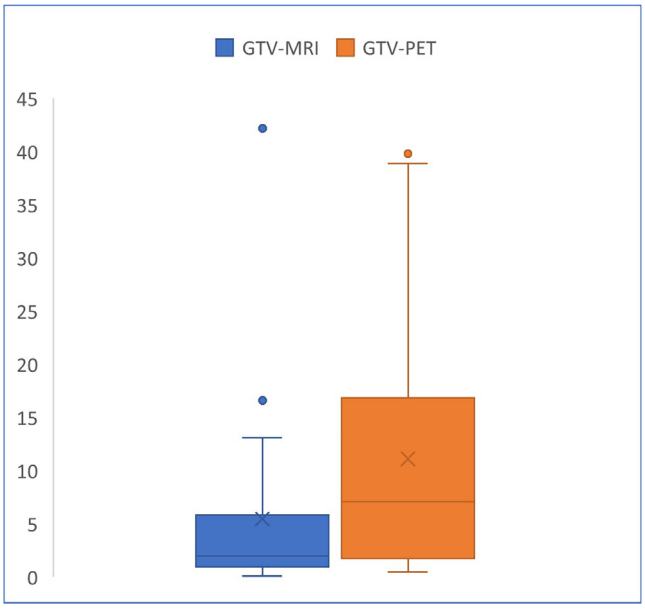

Figure 5 SUV_{mean} of the gross tumor volume (GTV) based on positron emission tomography (GTV-PET) and the GTV based on magnetic resonance imaging (GTV-MRI) measured in the 12 patients with maximum standardized uptake value (SUV_{max}) of GTV-PET located within the GTV-MRI. The median mean standardized uptake value (SUV_{mean}) was higher in GTV-MRI (7.45) than in GTV-PET (5.94), with a *P* value of .042.

underestimate the size of tumor foci, while Johnson et al[7] found that mpMRI fails to detect clinically significant tumor lesions in around 35% of patients.

^{68}Ga-PSMA PET enables the identification of areas of gross disease that are missed on CT. IMRT can be used to deliver a higher dose to areas with gross disease. Fig. 6 is an example of an IMRT plan and isodose results for (1) a patient with a rising PSA level after radical prostatectomy, planned without radiographic evidence of visible gross disease. Pelvic nodal and prostate bed volumes are prescribed at doses of 43 and 70 Gy, respectively. (2) The IMRT plan and isodose results for the patient who underwent mpMRI before planning. (3) The IMRT plan and isodose results for the patient who underwent ^{68}Ga-PSMA PET before planning. IMRT was used to focally increase the dose to the gross disease beyond 65 Gy while adequately sparing normal organs at risk. The dose-color wash displays the simulated dose on CT simulation scans, with a color scale of blue (43 Gy) to red (70 Gy).

In more than half of the patients, the GTV-PET was found to be at least 50% larger than the GTV-MRI, while in approximately one-fifth of the patients, the GTV-MRI was at least 50% larger than the GTV-PET. These findings validate the notion that GTVs in mpMRI are smaller than those in ^{68}Ga-PET/CT.[20] Consequently, these results suggest that incorporating margins in the GTV-MRI could potentially enhance the coverage of tumor lesions detected by ^{68}Ga-PSMA PET. Univariate analysis revealed a significant correlation between PSA level and the volume of GTV-MRI in terms of agreement in laterality between the 2 imaging techniques. This suggests that in patients with large tumor volumes in mpMRI, ^{68}Ga-PSMA PET/CT may provide limited additional information. Nevertheless, these patients are at high risk for lymph node or distant metastases.[25] ^{68}Ga-PSMA PET demonstrates high sensitivity and specificity in detecting lymph nodes, particularly for metastases smaller than 10 mm, making it valuable for lymph node staging.[26,27]

In addition, numerous studies have conducted a comparison between ^{68}Ga-PSMA tracers and the current standard of care, mpMRI, for the detection[28,29] and segmentation[20,21] of GTV. All research findings have consistently indicated that ^{68}Ga-PSMA PET imaging offers additional valuable insights. Nevertheless, a separate research team has documented that the visual interpretation of ^{68}Ga-PSMA PET images fails to detect clinically significant PCa in terms of microscopic lesions with an International Society of Urological Pathology grade greater than 1 in around 30% of patients.[30] The Prospective analysis of clinically significant prostate cancer detection with ^{18}F-DCFPyL PET/MRI compared to multiparametric MRI (ProStaPET) study prospectively evaluated the efficacy of 2-(3-(1-carboxy-5-[(6-[18F]fluoro-pyridine-3-carbonyl)-amino]-pentyl)-ureido)-pentanedioic acid (^{18}F-DCFPyL) PET and mpMRI in detecting PCa, with histopathology postsurgery serving as the gold standard for comparison.[31] The researchers reached the conclusion that the combination of PET/MR information does not surpass the use of mpMRI information alone.

Considering the results of center 1, PET identified a significantly higher number of intraprostatic PCa lesions with a notably larger volume compared with mpMRI. Additionally, the PET-GTV was also significantly larger in an external cohort. These findings align with previous

Table 1 Characteristics of gross tumor volumes defined on positron emission tomography data sets (gross tumor volume based on positron emission tomography) and magnetic resonance imaging data sets (gross tumor volume based on magnetic resonance imaging)

Patients	GTV-MRI (cm^3)	GTV-PET (cm^3)	PET SUV_{max}
1	3.1	9.8	3.88
2	3.8	10.1	6.47
3	13.1	38.9	9.64
4	2.5	1.2	12.11
5	0.6	10.7	3.7
6	42.2	39.8	3.08
7	1.6	1.9	5.04
8	0.2	2.5	6.45
9	3.6	12.7	14.78
10	10.5	24.6	2.43
11	2.7	8.3	15.76
12	1.3	3.7	10.91
13	0.1	1.2	46.34
14	2	1.6	3.23
15	1.3	1	59.4
16	7.9	21	7.79
17	0.6	7.1	8.46
18	0.4	0.5	5.75
19	0.7	2	5.76
20	16.6	35.9	7.6
21	2	4	3.09
22	1.8	1.2	3.01
23	13	24.8	13.3
24	1.6	2.8	6.72
25	3.5	11.1	2.05

The median GTV defined on PET images (GTV-PET = 4.16 cm^3) was larger than the median GTV defined on T2-weighted MRI (GTV-MRI = 3.5 cm^3). The difference between GTV-PET and GTV-MRI was significant ($P = .003$).
Abbreviations: GTV = gross tumor volume; MRI = magnetic resonance imaging; PET = positron emission tomography; SUV_{max} = maximum standardized uptake value.

studies that have compared ^{68}Ga-PSMA tracers with mpMRI.[14,29,32] Collectively, the results obtained from our investigation indicate that ^{68}Ga-PSMA PET/CT exhibits great potential as a valuable resource in directing focal therapy toward intraprostatic GTVs. Furthermore, it is plausible that this imaging technique may surpass the effectiveness of using MRI alone. Nevertheless, it is crucial to acknowledge the significance of mpMRI in this particular scenario because it offers supplementary data for certain patients. This is especially important considering that around 10% of intraprostatic GTVs do not exhibit PSMA expression.[33]

In our study, we noted that out of the 9 patients classified as high-risk, only 3 received ADT. This raises important questions regarding treatment decisions made for the remaining patients. Specifically, patient 10, who presented with a PSA level of 51 and a Gleason score of 8, did not receive ADT. The decision not to administer ADT in this case could be attributed to several factors. (1) Clinical assessment: the treating physician may have assessed the patient's overall health status, comorbidities, and personal preferences, which could have influenced the decision against initiating ADT. (2) Treatment protocols: there may be specific protocols or guidelines that prioritize ADT based on certain criteria that patient 10 did not meet despite having high-risk indicators. (3) Potential side effects: concerns regarding the side effects associated with ADT may have led to a more conservative approach in this particular case. (4) Alternative therapies: it is possible that alternative treatment options were considered more appropriate for patient 10 at the time of evaluation. (5) Multidisciplinary input: decisions regarding treatment often involve input from a multidisciplinary team; thus, differing opinions among specialists could also play a role in such decisions.

Current guidelines lack definitive recommendations regarding the suspension of ADT prior to PSMA-ligand PET imaging. Furthermore, there is a lack of guidance on the potential advantages of PSMA site stimulation through ADT. It is conceivable that ADT may also play a role in evaluating its impact on the metabolic response to treatment. Although the literature presents inconsistencies, the majority of studies indicate that short-term ADT enhances PSMA expression, thereby facilitating imaging under these conditions. Conversely, long-term ADT appears to diminish PSMA-ligand uptake as lesions shrink and partial volume effects become increasingly significant. There is a pressing need for comprehensive data emphasizing the evaluation of both castration-sensitive and castration-resistant models and patients, as well as the effects of short- and long-term ADT using various agents and mechanisms of action, alongside initial and late responses. Ultimately, a deeper understanding of the effects of ADT is essential, particularly in the context of preparing for systemic PSMA-ligand metabolic therapies. In conclusion, the temporal relationship between PSMA expression and the commencement of ADT may account for some of the variations in detection sensitivities observed in PSMA-ligand imaging. Nonetheless, there remains a substantial need to investigate the influence of medications and other factors at PSMA-ligand sites, likely through ongoing longitudinal studies and additional clinical research.

The expression of PSMA in benign prostatic hyperplasia (BPH) tissue and its related positive reaction are

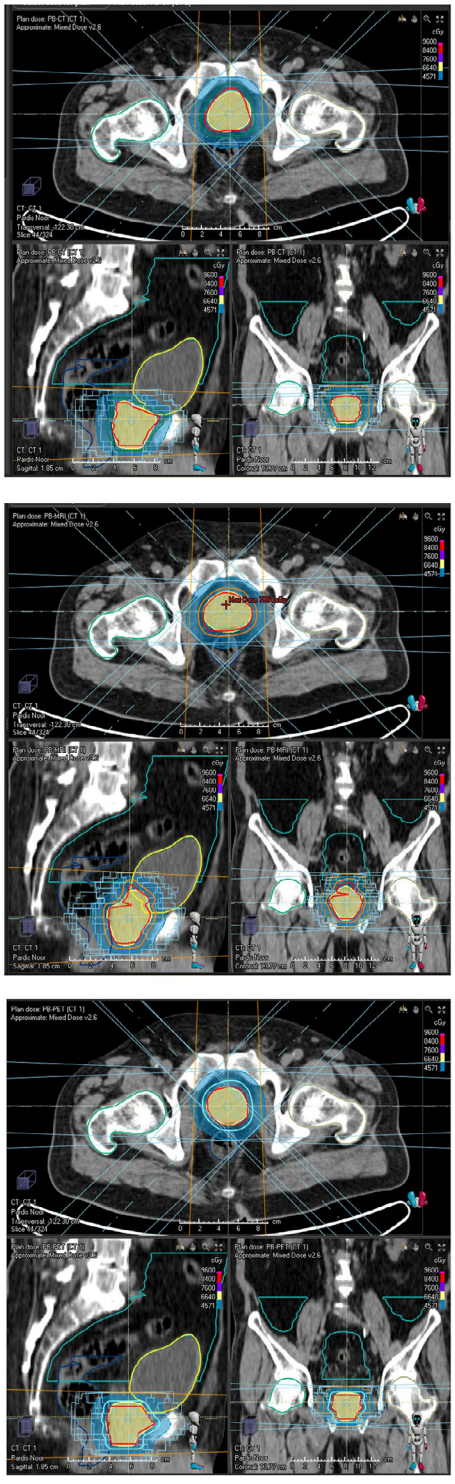

Figure 6 The top panel shows an example of an intensity modulated radiation therapy (IMRT) plan and isodose results for a patient with a rising prostate-specific antigen (PSA) level after a radical prostatectomy planned without radiographic evidence of visible gross disease. Pelvic nodal and prostate bed volumes are prescribed at doses of 43 and 70 Gy, respectively. The middle panel depicts the IMRT plan and isodose results for a patient who underwent multiparametric magnetic resonance imaging (MRI) before planning. The bottom panel shows an example of an IMRT plan and isodose results for a patient who underwent ^{68}Ga-prostate-specific membrane antigen positron emission tomography (PET) before planning. IMRT was used to focally increase the dose to gross disease beyond 65 Gy while adequately sparing normal organs at risk. The dose-color wash displays the simulated dose on a computed tomography (CT) simulation scan with a color scale varying from blue (43 Gy) to red (70 Gy).

crucial concerns for imaging diagnosis. In this study, 27 of 89 BPH cases (30.3%) showed false-positive uptake on ^{68}Ga-PSMA PET/CT, mimicking PCa. This highlights a significant limitation: PSMA is not cancer-specific and is also expressed in hyperplastic prostate tissue, leading to overdiagnosis. SUV_{max} thresholds (eg, a cutoff of 15 for 100% specificity) were proposed to mitigate this issue, but sensitivity dropped to 41%. Combining PSMA PET and mpMRI reduced but did not eliminate false positives (13% persisted). BPH-related PSMA uptake remains a major pitfall, as hyperplastic tissue expresses PSMA at levels overlapping with low-grade cancer. A study by Tang et al[34] found that even stringent PET/prostate imaging-reporting and data system (PI-RADS) criteria (both scores $\geq$ 4) could not fully exclude BPH false positives, underscoring the need for biopsy confirmation before radical treatments.

Privé et al[35] conducted a study comparing ^{18}F-PSMA-1007 PET with mpMRI in 23 patients, using histopathological analysis of surgical specimens as the gold standard. They observed similar results, further supporting the validity of our findings. Importantly, the NCCN risk groups assigned to the patients in our study were comparable between mpMRI and PSMA imaging, suggesting that the addition of PET imaging may not significantly alter the management of ADT in these patients.

A recent investigation conducted a comparative analysis between MRI and ^{18}F-DCFBC PET/CT alongside histopathological data following prostatectomy in 12 individuals. The researchers suggested the combined use of PSMA PET/CT and MRI to enhance the detection of clinically significant PCa.[17,25] Additionally, they quantified the GTV-PET SUV_{max} values encompassed within GTV-MRI and the extent of overlap between GTV-MRI and GTV-PET. Overall, the study found that mpMRI and ^{68}Ga-PSMA PET/CT exhibited concordance in around 50% of the patients.[25] Our investigation showed that the volume of GTV-PET was approximately double that of GTV-MRI, measuring 11.136 cm^3 and 5.468 cm^3, respectively. Moreover, the average coverage of GTV-MRI by the PTV from ^{68}Ga-PSMA PET/CT (66.1% GTV-MRI) exceeded the coverage of GTV-PET by the PTV from MRI (49.6% for GTV-MRI) (P value = .042). This observation aligns with earlier studies[36,37] that GTVs delineated using anatomic imaging tend to be smaller than those

outlined through functional imaging. It is essential to confirm potential clinical factors influencing agreement/disagreement between mpMRI and PSMA PET with accurate histopathological data in larger patient cohorts. Our findings demonstrate only partial agreement between the 2 imaging techniques. Until more definitive evidence on the diagnostic efficacy of ^{68}Ga-PSMA PET/CT becomes available, we recommend using mpMRI for identifying the involved lesions in PCa cases. In situations of uncertainty, such as the absence of GTV-MRI, a low Prostate Imaging Reporting and Data System score for GTV-MRI[38] or lack of agreement between GTV-MRI and histopathology following biopsy, ^{68}Ga-PSMA PET/CT may offer additional insights. Ensuring spatial alignment between GTV-PET and GTV-MRI could enhance diagnostic accuracy. It is important to note that GTV delineation based on DWI, DCE, and T2-weighted MRI may yield conflicting outcomes and limited agreement among observers,[39] while SUV-based GTV-PET delineation could serve as an objective tool for guiding focal dose escalation.[40] The distribution of the PET tracer, potentially leading to increased sensitivity and decreased specificity in detecting PCa with ^{68}Ga-PSMA PET/CT, may offer an additional rationale.

Nevertheless, Johnson et al[7] have determined that mpMRI has its limitations in detecting PCa foci, as it fails to identify around one-third of clinically significant foci.[39] However, a study has shown the potential of PSMA PET in conjunction with MRI to enhance the detection of clinically significant PCa.[41] In light of this, we propose the utilization of fused PET/MR images for accurate GTV delineation. Zhang et al[41] indicated that 83.3% of GTV-PET/MRI outcomes were superior to those of GTV-MRI. A prior investigation[42] also contended that MRI-based profiles typically underestimate tumor dimensions. Consequently, specialists suggest that sufficient radiation doses must be administered to the entire prostate during focal RT to avoid undertreatment in tumor-free regions. Gibson et al[43] proposed that using an enlarged GTV margin determined by mpMRI could potentially enhance the focus or therapeutic effect of PCa. Similar investigations conducted on various tumor sites have also demonstrated that the GTV-PET/MRI is larger compared with that obtained from GTV-MRI due to the additional biological information provided by PET. This additional information can help minimize the risk of errors in tumor location and influence the variability of GTV during RT.[41,42] Consequently, it is plausible to hypothesize that a larger GTV-PET/MRI could lead to a more comprehensive target acquisition, enabling adequate irradiation of the lesion and ultimately impacting the therapeutic outcome.

Recent comparative studies have systematically evaluated PSMA PET and mpMRI for intraprostatic tumor delineation using histopathological validation. Bettermann et al[20] demonstrated a superior volumetric correlation between PSMA PET (10.8 mL) and histopathology (10.4 mL) compared with mpMRI (4.5 mL; $P < .05$), with PSMA PET showing higher sensitivity (86% vs 58%) but slightly lower specificity (87% vs 94%). Notably, PSMA PET detected 133 tumor-positive quadrants that were missed by mpMRI. Complementary findings by Spohn et al[21] revealed that PSMA PET identified more lesions (159 vs 151) with larger median volumes (4.9 vs 2.8 mL; $P < .0001$) and superior bilateral lesion detection (71 vs 57; $P = .03$). Multivariate analysis confirmed MRI tumor volume as the sole significant predictor of laterality concordance ($P = .04$). These studies collectively established PSMA PET's clinical value in overcoming mpMRI's volumetric underestimation, particularly for intermediate/high-risk patients under the D'Amico classification, where combined imaging appears optimal for accurate GTV delineation.

Our study is constrained by several limitations, such as the modest sample size of 25 patients who underwent imaging on 2 distinct MRI and PET/CT scanners. There were various reconstruction techniques used along with a PET voxel size of 2.86 mm × 2.86 mm × 3.27 mm; nevertheless, the duration of bed positions ranged from 2 to 4 minutes among patients. Nevertheless, in this investigation, it proved unfeasible to consider all these discrepancies, leading us to make the assumption that the images and SUV values could be directly compared. Furthermore, it should be noted that the study has certain additional constraints. One such limitation is the absence of histology data derived from prostate tissue at the apex or the base. This is primarily due to the standard histology processing techniques employed, which necessitate the cutting of these sections in a parasagittal manner. Consequently, the inability to coregister these sections with the imaging data arises. Lastly, the potential impact of bowel and bladder motion on prostate movement between imaging acquisitions must be considered.[44] This challenge complicates the precise coregistration of MRI with PET/CT image data, potentially resulting in discrepancies in GTV delineation.

The discussion of false positives in PET is indeed crucial, as it has significant implications for diagnosis and treatment planning. False positives can occur due to various factors, including the physiological uptake of radiotracers in benign conditions, inflammation, or other nonmalignant processes that may mimic cancerous activity on PET scans. It is important to consider the clinical context and correlate PET findings with other diagnostic modalities, such as CT or MRI, as well as patient history and clinical symptoms. Additionally, using advanced imaging techniques and refined radiotracer selection can help mitigate the risk of false positives. In summary, while PET is a powerful tool in oncology, awareness and careful interpretation of potential false positives are essential for accurate diagnosis and effective patient management (Table E11). The inherent constraints of validation

criteria, particularly the restricted size variation observed in small lesions, have been addressed in prior discussions.[45] In contrast, ^{68}Ga-PSMA PET exhibits limitations in detecting small nodal metastases, particularly in regions with significant physiological uptake. Consistent with earlier studies, instances of false-negative results were observed in cases involving small metastases or when there was adjacent uptake from the bladder or urine.[46,47] Further CT urography proved beneficial in recognizing ^{68}Ga-PSMA PET results in proximity to the urinary system.[48]

Conclusions

In this investigation, we conducted a comparative analysis of individuals, comparing the effectiveness of ^{68}Ga-PSMA PET/CT and mpMRI in a substantial group of patients from 2 different centers. By employing reliable contouring methods, ^{68}Ga-PSMA PET demonstrated a greater number and larger size of tumor lesions compared with MRI. These findings have implications for determining the volume of focal RT targets, although they do not impact the NCCN risk group classification. Based on the findings, it would be more appropriate to suggest that while both imaging modalities have their merits, the data do not sufficiently support the necessity of using both in all cases in the RT planning process for PCa patients. Ongoing prospective trials are currently underway to assess the safety and therapeutic efficacy of focal RT using combined PSMA PET and mpMRI data.

Disclosures

None.

Declaration of Generative AI and AI-assisted technologies in the writing process

During the preparation of this work, the authors used OpenAI ChatGPT to enhance the English fluency of the manuscript and grammar checking. After using this tool/service, the authors reviewed and edited the content as needed and take full responsibility for the content of the publication.

Supplementary materials

Supplementary material associated with this article can be found in the online version at doi:10.1016/j.adro.2025.101821.

References

1. Bagheri H, Mahdavi SR, Geramifar P, et al. An update on the role of mpMRI and ^{68}Ga-PSMA PET imaging in primary and recurrent prostate cancer. *Clin Genitourin Cancer*. 2024;22:102076.
2. Yazdanpanah F, Houshi S, Hosseini M, et al. Machine learning based radiomics features of theranostics PET features in detection of Prostate cancer (PCa): A systematic review of 1703 patients. *J Nucl Med*. 2023;64(suppl 1):P1576.
3. Kasivisvanathan V, Rannikko AS, Borghi M, et al. MRI-targeted or standard biopsy for prostate-cancer diagnosis. *N Engl J Med*. 2018;378:1767-1777.
4. Turkbey B, Pinto PA, Mani H, et al. Prostate cancer: Value of multiparametric MR imaging at 3 T for detection-histopathologic correlation. *Radiology*. 2010;255:89-99.
5. Yakar D, Debats OA, Bomers JG, et al. Predictive value of MRI in the localization, staging, volume estimation, assessment of aggressiveness, and guidance of radiotherapy and biopsies in prostate cancer. *J Magn Reson Imaging*. 2012;35:20-31.
6. Mehrbanpajouh Q, Kamali-Asl A, Arabi H, Zaidi H. Automatic segmentation of prostate and its anatomical sub-regions from MR images using a novel ResUnet model. Paper presented at:. *2022 IEEE Nuclear Science Symposium and Medical Imaging Conference (NSS/MIC)*. Italy; 2022. November 5-12.
7. Johnson DC, Raman SS, Mirak SA, et al. Detection of individual prostate cancer foci via multiparametric magnetic resonance imaging. *Eur Urol*. 2019;75:712-720.
8. Priester A, Natarajan S, Khoshnoodi P, et al. Magnetic resonance imaging underestimation of prostate cancer geometry: Use of patient specific molds to correlate images with whole mount pathology. *J Urol*. 2017;197:320-326.
9. Hofman MS, Lawrentschuk N, Francis RJ, et al. Prostate-specific membrane antigen PET-CT in patients with high-risk prostate cancer before curative-intent surgery or radiotherapy (proPSMA): A prospective, randomised, multicentre study. *Lancet*. 2020;395:1208-1216.
10. Dorri Giv M, Arabi H, Naseri S, et al. Evaluation of the prostate cancer and its metastases in the [68 Ga]Ga-PSMA PET/CT images: Deep learning method vs. conventional PET/CT processing. *Nucl Med Commun*. 2024;45:974-983.
11. Arabi H, Zaidi H. Recent advances in positron emission tomography/magnetic resonance imaging technology. *Magn Reson Imaging Clin N Am*. 2023;31:503-515.
12. Dadgar H, Pashazadeh A, Norouzbeigi N, et al. Targeted radioligand therapy: Physics and biology, internal dosimetry and other practical aspects during ^{177}Lu/^{225}Ac treatment in neuroendocrine tumors and metastatic prostate cancer. *Theranostics*. 2025;15:4368-4397.
13. Eder M, Schäfer M, Bauder-Wüst U, et al. 68Ga-complex lipophilicity and the targeting property of a urea-based PSMA inhibitor for PET imaging. *Bioconjug Chem*. 2012;23:688-697.
14. Eiber M, Maurer T, Souvatzoglou M, et al. Evaluation of hybrid ^{68}Ga-PSMA ligand PET/CT in 248 patients with biochemical recurrence after radical prostatectomy. *J Nucl Med*. 2015;56:668-674.
15. Ceci F, Uprimny C, Nilica B, et al. (68)Ga-PSMA PET/CT for restaging recurrent prostate cancer: Which factors are associated with PET/CT detection rate? *Eur J Nucl Med Mol Imaging*. 2015;42:1284-1294.
16. Afshar-Oromieh A, Zechmann CM, Malcher A, et al. Comparison of PET imaging with a (68)Ga-labelled PSMA ligand and (18)F-choline-based PET/CT for the diagnosis of recurrent prostate cancer. *Eur J Nucl Med Mol Imaging*. 2014;41:11-20.
17. Rowe SP, Gage KL, Faraj SF, et al. ^{18}F-DCFBC PET/CT for PSMA-based detection and characterization of primary prostate cancer. *J Nucl Med*. 2015;56:1003-1010.
18. Singh M, Katdare A, Ghosh S, et al. PSMA-PET guided intra-prostatic boost in prostate SBRT (PROBE): A phase II trial. *Int J Radiat Oncol Biol Phys*. 2025. forthcoming.

19. Liu LL, Zhu LL, Lu ZG, et al. Variability of radiotherapy volume delineation: PSMA PET/MRI and MRI based clinical target volume and lymph node target volume for high-risk prostate cancer. *Cancer Imaging*. 2023;23:1.
20. Bettermann AS, Zamboglou C, Kiefer S, et al. [^{68}Ga-]PSMA-11 PET/CT and multiparametric MRI for gross tumor volume delineation in a slice by slice analysis with whole mount histopathology as a reference standard - Implications for focal radiotherapy planning in primary prostate cancer. *Radiother Oncol*. 2019;141:214-219.
21. Spohn SKB, Kramer M, Kiefer S, et al. Comparison of manual and semi-automatic [^{18}F]PSMA-1007 PET based contouring techniques for intraprostatic tumor delineation in patients with primary prostate cancer and validation with histopathology as standard of reference. *Front Oncol*. 2020;10:600690.
22. Salembier C, Villeirs G, De Bari B, et al. ESTRO ACROP consensus guideline on CT- and MRI-based target volume delineation for primary radiation therapy of localized prostate cancer. *Radiother Oncol*. 2018;127:49-61.
23. Zamboglou C, Klein CM, Thomann B, et al. The dose distribution in dominant intraprostatic tumour lesions defined by multiparametric MRI and PSMA PET/CT correlates with the outcome in patients treated with primary radiation therapy for prostate cancer. *Radiat Oncol*. 2018;13:65.
24. Pucar D, Hricak H, Shukla-Dave A, et al. Clinically significant prostate cancer local recurrence after radiation therapy occurs at the site of primary tumor: Magnetic resonance imaging and step-section pathology evidence. *Int J Radiat Oncol Biol Phys*. 2007;69:62-69.
25. Zamboglou C, Wieser G, Hennies S, et al. MRI versus ^{68}Ga-PSMA PET/CT for gross tumour volume delineation in radiation treatment planning of primary prostate cancer. *Eur J Nucl Med Mol Imaging*. 2016;43:889-897.
26. Mottet N, Bellmunt J, Bolla M, et al. EAU-ESTRO-SIOG guidelines on prostate cancer. Part 1: Screening, diagnosis, and local treatment with curative intent. *Eur Urol*. 2017;71:618-629.
27. Cook GJR, Kulkarni M, Warbey VS. PSMA PET/CT imaging for primary staging of intermediate and high-risk prostate cancer. *BJU Int*. 2019;124:357-358.
28. Meißner S, Janssen JC, Prasad V, et al. Accuracy of standard clinical 3T prostate MRI for pelvic lymph node staging: Comparison to ^{68}Ga-PSMA PET-CT. *Sci Rep*. 2019;9:10727.
29. Chen M, Zhang Q, Zhang C, et al. Combination of ^{68}Ga-PSMA PET/CT and multiparametric MRI improves the detection of clinically significant prostate cancer: A lesion-by-lesion analysis. *J Nucl Med*. 2019;60:944-949.
30. Emmett L, Buteau J, Papa N, et al. The additive diagnostic value of prostate-specific membrane antigen positron emission tomography computed tomography to multiparametric magnetic resonance imaging triage in the diagnosis of prostate cancer (PRIMARY): A prospective multicentre study. *Eur Urol*. 2021;80:682-689.
31. Zamboglou C, Bettermann AS, Gratzke C, et al. Uncovering the invisible-prevalence, characteristics, and radiomics feature-based detection of visually undetectable intraprostatic tumor lesions in (68)GaPSMA-11 PET images of patients with primary prostate cancer. *Eur J Nucl Med Mol Imaging*. 2021;48:1987-1997.
32. Bodar YJL, Zwezerijnen BGJC, van der Voorn PJ, et al. Oprea-lager, prospective analysis of clinically significant prostate cancer detection with [^{18}F]DCFPyL PET/MRI compared to multiparametric MRI: A comparison with the histopathology in the radical prostatectomy specimen, the ProStaPET study. *Eur J Nucl Med Mol Imaging*. 2022;49:1731-1742.
33. Ferraro DA, Becker AS, Kranzbühler B, et al. Diagnostic performance of (68)Ga-PSMA-11 PET/MRI-guided biopsy in patients with suspected prostate cancer: a prospective single-center study. *Eur J Nucl Med Mol Imaging*. 2021;48:3315-3324.
34. Tang W, Tang Y, Qi L, et al. Benign prostatic hyperplasia-related false-positive of prostate-specific membrane antigen-positron emission tomography in the diagnosis of prostate cancer: The Achilles' heel of biopsy-free radical prostatectomy? *J Urol*. 2023;210:845-855.
35. Privé BM, Israël B, Schilham MGM, et al. Evaluating F-18-PSMA-1007-PET in primary prostate cancer and comparing it to multiparametric MRI and histopathology. *Prostate Cancer Prostatic Dis*. 2021;24:423-430.
36. Milker-Zabel S, Zabel-du Bois A, Henze M, et al. Improved target volume definition for fractionated stereotactic radiotherapy in patients with intracranial meningiomas by correlation of CT, MRI, and [68Ga]-DOTATOC-PET. *Int J Radiat Oncol Biol Phys*. 2006;65:222-227.
37. Shepherd T, Teras M, Beichel RR, et al. Comparative study with new accuracy metrics for target volume contouring in PET image guided radiation therapy. *IEEE Trans Med Imaging*. 2012;31:2006-2024.
38. Barentsz JO, Richenberg J, Clements R, et al. ESUR prostate MR guidelines 2012. *Eur Radiol*. 2012;22:746-757.
39. Rischke HC, Nestle U, Fechter T, et al. 3 Tesla multiparametric MRI for GTV-definition of Dominant Intraprostatic lesions in patients with prostate cancer—An interobserver variability study. *Radiat Oncol*. 2013;8:183.
40. Maroufpour S, Aryana K, Nasseri S, Fazeli Z, Arabi H, Momennezhad M. Validation of dosimetry programs (Olinda & IDAC) for evaluation of absorbed dose in ^{177}LuPSMA therapy of metastatic castration-resistant prostate cancer (mCRPC) using Monte Carlo simulation. *EJNMMI Phys*. 2024;11:102.
41. Zhang YN, Lu ZG, Wang SD, et al. Gross tumor volume delineation in primary prostate cancer on ^{18}F-PSMA-1007 PET/MRI and ^{68}Ga-PSMA-11 PET/MRI. *Cancer Imaging*. 2022;22:36.
42. Ma JT, Han CB, Zheng JH, et al. Hybrid PET/MRI-based delineation of gross tumor volume in head and neck cancer and tumor parameter analysis. *Nucl Med Commun*. 2017;38:642-649.
43. Gibson E, Bauman GS, Romagnoli C, et al. Toward prostate cancer contouring guidelines on magnetic resonance imaging: Dominant lesion gross and clinical target volume coverage via accurate histology fusion. *Int J Radiat Oncol Biol Phys*. 2016;96:188-196.
44. Moiseenko V, Liu M, Kristensen S, Gelowitz G, Berthelet E. Effect of bladder filling on doses to prostate and organs at risk: A treatment planning study. *J Appl Clin Med Phys*. 2006;8:55-68.
45. Jilg CA, Drendel V, Rischke HC, et al. Diagnostic accuracy of Ga-68-HBED-CC-PSMA-ligand-PET/CT before salvage lymph node dissection for recurrent prostate cancer. *Theranostics*. 2017;7:1770-1780.
46. Fennessy N, Lee J, Shin J, et al. Frusemide aids diagnostic interpretation of (68)Ga-PSMA positron emission tomography/CT in men with prostate cancer. *J Med Imaging Radiat Oncol*. 2017;61:739-744.
47. Iravani A, Hofman MS, Mulcahy T, et al. ^{68}Ga PSMA-11 PET with CT urography protocol in the initial staging and biochemical relapse of prostate cancer. *Cancer Imaging*. 2017;17:31.
48. Fendler WP, Calais J, Eiber M, et al. Assessment of 68Ga-PSMA-11 PET Accuracy in localizing recurrent prostate cancer: A prospective single-arm clinical trial. *JAMA Oncol*. 2019;5:856-863.